

Effective potential for Polyakov loops from a center symmetric effective theory in three dimensions

Dominik Smith^{a,b,c}

^a*Institut für Theoretische Physik, Johann Wolfgang Goethe-Universität,
Max-von-Laue-Str. 1, 60438 Frankfurt am Main, Germany*

^b*Frankfurt International Graduate School for Science (FIGGS),
Ruth-Moufang-Str. 1, 60438 Frankfurt am Main, Germany*

^c*Helmholtz Research School for Quark Matter Studies (H-QM),
Max-von-Laue-Str. 1, 60438 Frankfurt/Main, Germany*

(Dated: October 23, 2018)

We present lattice simulations of a center symmetric dimensionally reduced effective field theory for SU(2) Yang Mills which employ thermal Wilson lines and three-dimensional magnetic fields as fundamental degrees of freedom. The action is composed of a gauge invariant kinetic term, spatial gauge fields and a potential for the Wilson line which includes a “fuzzy” bag term to generate non-perturbative fluctuations. The effective potential for the Polyakov loop is extracted from the simulations including all modes of the loop as well as for cooled configurations where the hard modes have been averaged out. The former is found to exhibit a non-analytic contribution while the latter can be described by a mean-field like *ansatz* with quadratic and quartic terms, plus a Vandermonde potential which depends upon the location within the phase diagram.

PACS numbers: 12.38.-t, 12.38.Gc, 12.38.Mh

I. INTRODUCTION

QCD at temperatures $T \simeq 200 \text{ MeV} - 1 \text{ GeV}$ exhibits only partial deconfinement and, moreover, perturbation theory fails to reproduce some thermodynamic quantities such as the equation of state [1]. Several authors [2–6] have suggested that in this regime a more appropriate effective description is not in terms of quasi-particles but in terms of the thermal Wilson line

$$\mathbf{L}(\mathbf{x}) = \mathcal{Z}_R^{-1} \mathcal{P} \exp \left(ig \int_0^{1/T} d\tau A_0(\mathbf{x}, \tau) \right), \quad (1)$$

and the spatial components of the gauge field. The operator A_0 from eq. (1) is defined on four dimensional euclidean space-time while $\mathbf{L}(\mathbf{x})$ is a matrix-valued field in space. \mathcal{Z}_R denotes a renormalization constant, which can be calculated in different representations of \mathbf{L} [3, 7]. We take \mathbf{L} to be in the fundamental representation here. In such a framework, the deconfined phase is not a free gas, but rather a condensate of spin-like operators

$$\ell(\mathbf{x}) = \frac{1}{N} \text{tr} \mathbf{L}(\mathbf{x}), \quad (2)$$

called *Polyakov loops*. The volume averaged expectation value of this operator is an order parameter for the deconfining phase transition in the limit of infinitely massive quarks [7]. In contrast to ferromagnetism, the high temperature phase is the ordered phase where a global symmetry is spontaneously broken.

We perform lattice simulations of an effective theory

in three dimensions defined in the continuum by [5]

$$\begin{aligned} \mathcal{L}^{\text{eff}} = & \frac{1}{2} \text{tr} G_{ij}^2 + \frac{T^2}{g^2} \text{tr} |\mathbf{L}^\dagger D_i \mathbf{L}|^2 \\ & - \frac{2}{\pi^2} T^4 \sum_{n \geq 1} \frac{1}{n^4} |\text{tr} \mathbf{L}^n|^2 + B_f T^2 |\text{tr} \mathbf{L}|^2. \end{aligned} \quad (3)$$

All fields in (3) are functions of \mathbf{x} only. G_{ij} is the magnetic field strength. The second term is the contribution from electric fields since in the three-dimensional theory, for *arbitrary* A_0 , \mathbf{E} is given by [5]

$$\mathbf{E}_i(\mathbf{x}) = \frac{T}{ig} \mathbf{L}^\dagger(\mathbf{x}) \mathbf{D}_i(\mathbf{x}) \mathbf{L}(\mathbf{x}). \quad (4)$$

The potential $\sim -\sum_{n \geq 1} |\text{tr} \mathbf{L}^n|^2 / n^4$ for the Wilson line \mathbf{L} is obtained by computing the one-loop fluctuation determinant in a constant background \mathbf{A}_0 (or \mathbf{L}) field [8]. It is evidently minimized by the perturbative vacuum $\langle \mathbf{L} \rangle = \mathbf{1}$ (times a phase), for any T . To generate a phase transition in infinite volume, refs. [4, 5] suggested to add non-perturbative contributions such as $B_f T^2 |\text{tr} \mathbf{L}|^2$, with B_f a “fuzzy” bag constant (see, also, refs. [9]). The “fuzzy bag” dominates at sufficiently low temperature and induces a transition to a confined phase with $\langle \text{tr} \mathbf{L} \rangle = 0$.

The three-dimensional effective theory (3) is valid only over distance scales larger than $1/T$ and is non-renormalizable. A related renormalizable 3D theory, which in a rough sense corresponds to a linear sigma model version of (3) has been formulated in refs. [6] (see also ref. [10]). These effective theories respect the global Z(N) center symmetry of the four-dimensional Euclidean SU(N) Yang-Mills theory. This allows for non-perturbatively large fluctuations of the Wilson line and it is interesting to investigate whether such an extension

of high-temperature perturbation theory is sufficient to describe the properties of hot Yang-Mills even close to the temperature for deconfinement.

We note that there have been various attempts at extracting through numerical simulations a three-dimensional effective action which reproduces the long-range properties of the underlying four-dimensional Yang-Mills theory [11]. Here, our approach is different (mostly because we do not aim at matching the couplings of the 3d theory yet). We shall focus on extracting an effective potential and analysing its structure from the 3d theory itself.

II. LATTICE ACTION

Our present simulations have been performed for gauge group $SU(2)$. The structure of this group is simpler than that of $SU(3)$, and thus allows for much higher numerical precision but exhibits the qualitative features which we are interested in, namely a deconfining phase transition and non-perturbative fluctuations between center-symmetric states. The lattice action is of the form

$$S = \beta \sum_{\square} \left(1 - \frac{1}{2} \text{Re tr } \mathbf{U}_{\square}\right) - \frac{1}{2} \beta \sum_{\langle ij \rangle} \text{tr} (\mathbf{L}_i \mathbf{U}_{ij} \mathbf{L}_j^{\dagger} \mathbf{U}_{ij}^{\dagger} + \text{h.c.}) - m^2 \sum_i |\text{tr } \mathbf{L}_i|^2. \quad (5)$$

The first term is the standard Wilson action for the magnetic fields in three dimensions; the sum runs over all spatial plaquettes. We have checked that our implementation reproduces the plaquette expectation values published in ref. [12]. The second term is a kinetic term for the Wilson line corresponding to the electric fields in three dimensions. Here, the sum runs over all links connecting nearest neighbor sites and the gauge links U_{ij} ensure gauge invariance. The third term is a mass term for the trace of the Wilson line which combines the $n = 1$ contribution to the one-loop potential with the non-perturbative "fuzzy" bag contribution. Contributions from larger n have been dropped¹. We have previously performed simulations of a simplified version of (5) without magnetic fields in ref. [13]. For $m^2 = 0$, and without magnetic fields, our code reproduces free energy measurements from refs. [14] but differs slightly from the older work of ref. [15] which used smaller lattices and lower statistics.

We employ the standard Metropolis algorithm to generate a thermal ensemble of configurations. The lattice is

updated sequentially. To reduce autocorrelations and accelerate thermalization we include over-relaxation sweeps where the Metropolis trial steps are taken deterministically in a way that approximately inverts the action with respect to its minimum [16] (exact non-stochastic over-relaxation, as well as heat bath updating, is not possible due to the non-linear term in the action). For the Wilson lines, sweeps are performed by applying 5 random Metropolis hits and 2 over-relaxed Metropolis hits on each site before moving to the next site. For the gauge links we mix 8 random Metropolis hits with 3 over-relaxed hits per step. We treat the Wilson line \mathbf{L} equivalent to the single time-like link of a $N_{\tau} = 1$ gauge theory, for which ref. [17] discussed the different treatments of the time-like boundary conditions which are possible. We employ the so-called *time-plaquette-double-counting* scheme, where the U_{ij} possess staples in the positive as well as the negative time-direction, which happen to give equal contributions. The result is an additional factor two in front of the kinetic nearest neighbour contribution to the action, when updating the spatial links U_{ij} .

All sample sizes quoted here are taken to be statistically independent measurements. We have estimated the integrated autocorrelation time by using the *binning* method described in ref. [18]. The method consists of grouping fixed numbers of successive data points, obtaining a new set of points which contains the average values of each group and then comparing the variances of the old and the new set. We found that on the order of 25 configurations must be discarded between measurements far from the phase boundary and on the order of 400 configurations at the phase boundary on the largest ($N_s = 24$) lattice (we refrain from showing any figures). We found that the thermal relaxation time within the Monte Carlo time series of measurements is roughly of the same order not too close to the phase boundary.

We have obtained error estimates for the numerical results presented in this work. The errors of the phase boundary presented in Fig. 1 are given by the finite resolution in β and m^2 respectively. The errorbars for the coefficients presented in Figs. 3,5,10, 11,12,13 and 14 result from the χ^2 fit. In Fig. 16 we include the statistical errorbar for the Polyakov expectation value. In all of these cases, the errorbar is often smaller than the point size and thus cannot be seen in the respective figure. The results presented in Fig. 6 are absolute numbers and are presented without errorbars. The potentials shown in Figs. 2, 4, 7, 8, 9 and 15 are obtained from a histogram, which is obtained without statistical errorbars. However, the errors can be estimated from the fluctuations which are visible in the figures. We have obtained a data set of sufficient size, such that fluctuations are strongly suppressed for a large region surrounding the minimum of the potential.

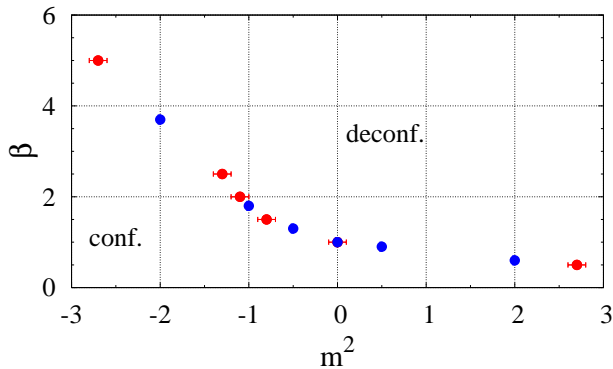
¹ Terms corresponding to $n > 1$ are suppressed by $1/n^4$. They are most important when the Polyakov loop is near unity; there, the full sum, $\sum 1/n^4 = \pi^4/90 = 1.08232$, is about 8.2% larger than the leading term.

III. RESULTS

A. Phase diagram

To determine the phase diagram of the theory we measure the expectation value of the Polyakov loop $\ell(\mathbf{x}) = \frac{1}{2}\text{tr} \mathbf{L}(\mathbf{x})$ and the inverse correlation length $m_\xi = 1/\xi$ as functions of the couplings m^2 and β . There is a line of phase transitions in the $\beta - m^2$ plane separating the region where the expectation value of the Polyakov loop vanishes (the Z(2) symmetric phase at low β , m^2) from the Z(2) broken phase at large β or m^2 (see fig. 1). The transition is of second order since the inverse correlation length m_ξ on the phase boundary extrapolates to zero in the infinite volume limit [13] as long as β is not too large². It appears that the order of the phase transition changes to first order at roughly $\beta > 3.0$. This may signal a breakdown of this model as an effective description of 4D Yang Mills in the extreme weak coupling limit (for a discussion of this issue see Appendix B).

Confinement is realized in distinct ways. At small β and vanishing m^2 we find $\langle \ell \rangle = 0.0$ because the Wilson line $\mathbf{L}(\mathbf{x})$ averages to zero from random fluctuations over the whole group manifold. For large β and negative m^2 (corresponding to the upper left region in fig. 1), we find a non-trivial Z(2) symmetric phase, where the Wilson lines fluctuate only outside of the group center ($\mathbf{L}(\mathbf{x}) = i\tau_3$ or rotations thereof), and the trace of \mathbf{L} vanishes locally for each site³. Unlike for the model without gauge fields studied in ref. [13] however, there is no global alignment of the Wilson lines in the confined phase and no sharp phase boundary separating the two types of confined vacua.



² The second order phase transition is further confirmed by the potentials described in later sections

³ In other words, the distributions of the eigenvalues λ_1 and λ_2 , which are gauge invariant, peak about ± 1 . That distinct confined phases with different eigenvalue structure can also arise in 4d models of Polyakov loops coupled to gauge fields, was shown in refs. [19]

FIG. 1: The phase boundary in the $\beta - m^2$ plane. The Z(2)-broken phase corresponds to the upper-right region.

B. Effective potential

We are interested in the distribution of the eigenvalues λ_1, λ_2 of the Wilson line \mathbf{L} over the thermal ensemble of field configurations at each site. Here, we shall focus on the potential for the average of λ_1 and λ_2 :

$$\rho(\mathbf{x}) = \frac{1}{2} |\lambda_1(\mathbf{x}) + \lambda_2(\mathbf{x})| \quad , \quad (6)$$

which for SU(2) is nothing but the absolute value of the Polyakov loop, $\rho = \sqrt{\ell^2}$. From the probability distribution for ρ we define an effective potential⁴ via

$$V_{\text{eff}}(\rho) = -\log P(\rho) \quad . \quad (7)$$

We normalize the probability density $P(\rho)$ over the interval $[0,1]$ which fixes the constant in the potential. This also factors out the volume dependence. The partition function can thus be written as

$$Z = \int d\rho e^{-N_s^3 V_{\text{eff}}(\rho)} \quad . \quad (8)$$

In our definition, therefore, $V_{\text{eff}}(\rho)$ is dimensionless as it absorbs the volume a^3 of a lattice cell and, implicitly, a factor of $1/T$ (because we employ a 3d theory).

Below, we shall show that in the weak-coupling regime (large β , small m^2) a non-analytic contribution $\sim \sqrt{\ell^2}$ to the effective potential arises dynamically. It is distinct from the Vandermonde potential $V_{\text{Vdm}} = -\frac{1}{2} \log(1 - \ell^2)$ generated by the SU(2) group measure, and from the "bare" potential $\sim -m^2 \ell^2$ which is included in the action (5). We find that for a broad range of the couplings β and m^2 the potential has the form

$$V_{\text{fit}}(\rho) = -\frac{1}{2} \log(1 - \rho^2) + a - b\rho + c\rho^2 \quad . \quad (9)$$

Note that the term proportional to $\rho \equiv \sqrt{\ell^2}$ of course does not break the Z(2) symmetry explicitly, and is not to be confused with a Z(2) background field $\sim -h\ell$ corresponding to (heavy) dynamical quarks in the fundamental representation (note also that the coefficient a is just a normalization and is not of any physical significance).

All measurements presented here were performed on a $N_s = 24$ cubic lattice. However, using smaller lattices we have checked that the coefficients a, b, c from (9) do not change much with volume if $N_s \geq 12$. $N_s = 24$ appears to be a good approximation to the infinite

⁴ Strictly speaking, what is studied here is what by usual naming conventions is known as the "constraint effective potential".

volume limit where, as indicated in eq. (8), one expects the potential to be volume independent (this holds even close to the phase boundary where correlation lengths diverge). 5000 independent lattice configurations were generated for each combination of β, m^2 .

We first consider the case without potential, $m^2 = 0$. The phase transition occurs at $\beta_C \approx 0.9$ for this case. Below the phase transition point we find that the potential defined via eq. (7) coincides with the Vandermonde potential V_{Vdm} , hence $a = b = c = 0$ within numerical precision. This is shown in fig. 2. On the other hand, for

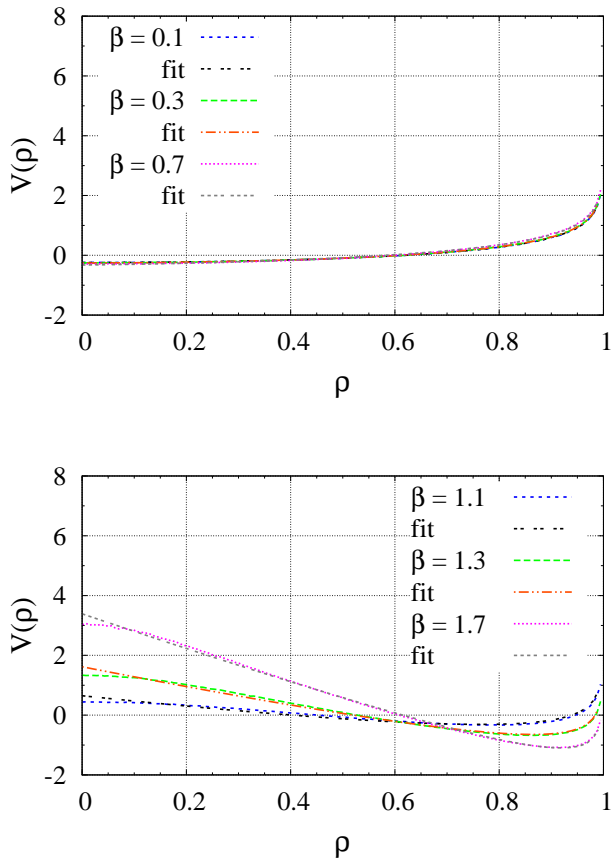


FIG. 2: Effective potential for $\rho = \sqrt{\ell^2}$ at $m^2 = 0$ for various values of β fitted with the *ansatz* (9). For $\beta < \beta_C$ (top) one sees only the group integration measure. Above β_C spontaneous breaking of $Z(2)$ is evident.

$\beta > \beta_C$ both coefficients a and b from eq. (9) turn non-zero. The quadratic coefficient c does not appear since $m^2 = 0$. The coefficient b appears to arise purely from the dynamics of fluctuations. Its behavior is shown in fig. 3.

The *ansatz* (9) also works for $m^2 \neq 0$ when β is not too large. We have confirmed this for a broad range of m^2 for several fixed values of β . Explicit results for $\beta = 2.0$ are shown in fig. 4. The coefficient c of the quadratic term appears to depend linearly on the square mass from the

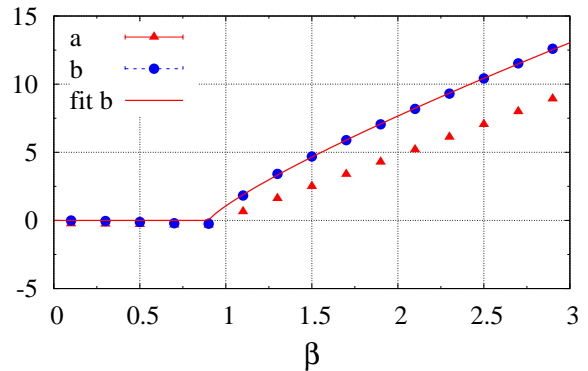


FIG. 3: Coefficients of the effective potential $V(\rho)$ for $m^2 = 0$ as a function of β . Below β_C there is no deviation from the Vandermonde potential. Above β_C one sees a non-analytic contribution. (A discussion of the fit-curve is found in Appendix A.)

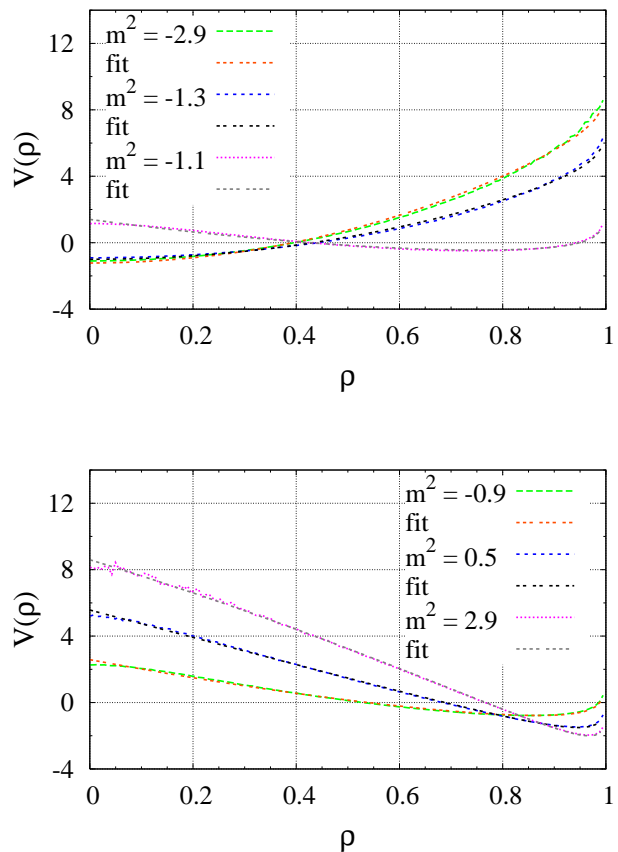


FIG. 4: Effective potential for ρ at $\beta = 2.0$ for various values of m^2 above and below the phase transition, fitted with the *ansatz* (9).

bare potential, $c \sim -m^2$, except exactly at the phase

transition where it changes discontinuously.

However, we again observe that above the phase transition point the dynamics generates a non-analytic contribution to the potential for the Polyakov loop proportional to $\rho \equiv \sqrt{\ell^2}$. For illustration, we show the m^2 dependence of a, b, c for $\beta = 1.0$ and $\beta = 2.0$ in fig. 5. A detailed discussion of the dependence of a, b, c on β and m^2 is given in appendix A. The main point here is that the Vandermonde contribution to the effective potential does not depend on β and m^2 , and that the effective potential obtained from a histogram of $\rho(\mathbf{x})$ at each lattice site is different from a Landau-Ginzburg type mean-field theory for the Polyakov loop. In the next section we shall see that when the field configurations are “cooled” to remove short wavelength fluctuations, that in fact one does obtain a potential that resembles mean field theory, but with a coefficient multiplying the Vandermonde potential which depends on β and m^2 .

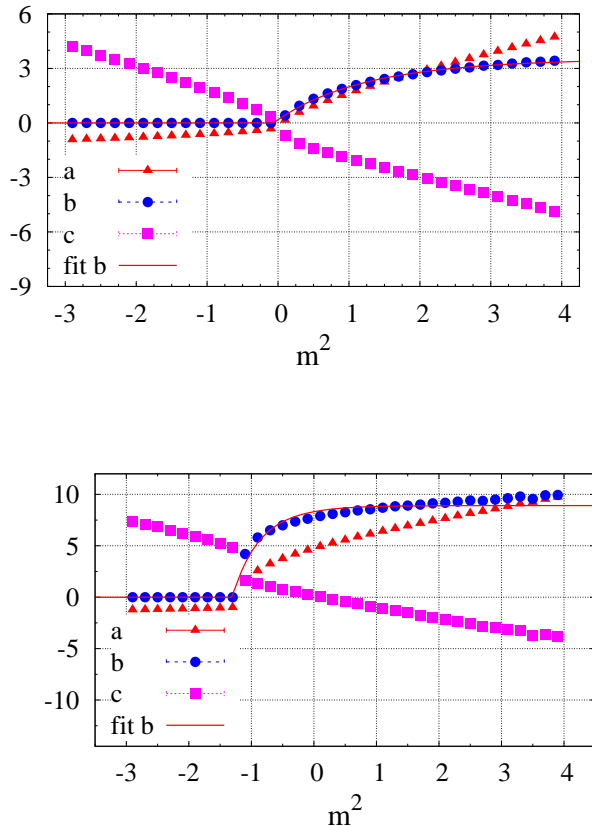


FIG. 5: Coefficients of $V(\rho)$ for $\beta = 1.0$ (top) and $\beta = 2.0$ (bottom) as functions of m^2 . The non-analytic contribution sets in at the phase transition.

C. Effective potential for block spins

To obtain a potential for the *long wavelength modes* we average the Polyakov loop field over small cubes of side-length k before histogramming. This eliminates the short wavelength spatial field modes. We calculate *blockspin averages* defined as

$$\bar{\ell}_i^{(k)} = \frac{1}{k^3} \sum_{\vec{n}} \frac{1}{2} \text{tr} \mathbf{L}(\vec{i} + \vec{n}), \quad (10)$$

$$\vec{n} = (0, 0, 0) \dots (k, k, k).$$

We have investigated the cases $k = 2, 3, 4$. Blockspins were measured on 2500 independent configurations for each combination of β, m^2 . As one expects from the central limit theorem (at least in the region far from the phase boundary where screening masses are large and individual lattice sites fluctuate independently), with increasing k the potential becomes more symmetric and peaked around the actual expectation value (see fig. 7). In what follows, we take the configurations for $k = 3$ as a good approximation for the long distance sector. To see this consider fig. 6. At $k = 3$ the minimum of the fitted effective potential from eq. (11) differs at most by $\simeq 0.03$ from the numerical result for the Polyakov loop expectation value $\langle \ell \rangle$. This maximal deviation occurs exactly at the phase transition point. Here, within our numerical precision, $k = 4$ does not do significantly better. Away from the phase transition, $k = 3$ differs less than $\simeq 0.01$ from the numerical value of $\langle \ell \rangle$. $k = 4$ does slightly better but reduces our statistics significantly. All results presented below appear to be stable when going from $k = 3$ to $k = 4$ (we will discuss an explicit example below). We refrain from discussing $k = 2$ in detail here as it appears that contributions from the short range fluctuation have not yet been completely eliminated.

The *ansatz* (9) is no longer applicable for the long wavelength modes. The blockspin averaging appears to suppress the non-analytic term in the potential in most parts of the phase diagram (some possible exceptions are discussed below). It appears that over a broad range of β and m^2 the potential can be described fairly well by a form analogous to mean field models, with quadratic and quartic terms [20]. However, for a good fit to the extracted potential one needs to include an additional parameter d_0 into the fit function which varies with β and m^2 , and which multiplies the Vandermonde potential. So, finally, the form which we use to model our data is

$$V(\rho) = -d_0 \frac{1}{2} \log(1 - \rho^2) + d_1 + d_2 \rho^2 + d_4 \rho^4. \quad (11)$$

Here, a linear term is not included. We also point out that the quartic term arises from the dynamics of fluctuations as such a contribution is not included in the “bare” action (5). Explicit results for the numerical potential and for the fit via eq. (11), for different values of m^2 in the confined and deconfined phases and fixed

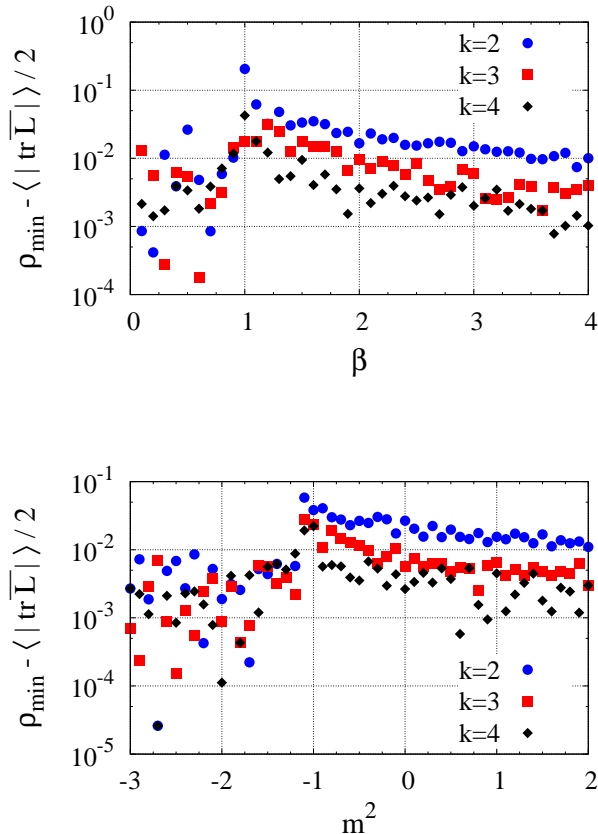


FIG. 6: The difference of Polyakov loop expectation value and minimum of effective potential after “cooling” for $k = 2, 3, 4$ at $m^2 = 0.0$ as a function of β (top) and at $\beta = 2.0$ (bottom) as a function of m^2 . The peaks correspond to the phase transition point.

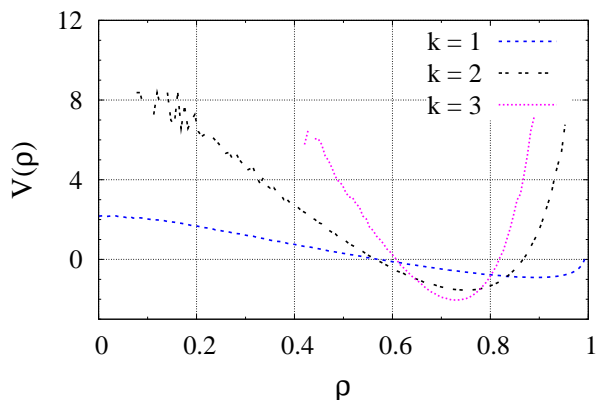


FIG. 7: Blockspin averages for $\beta = 1.5$, $m^2 = 0.0$. As k increases the potential peaks more sharply about the expectation value.

$\beta = 2.0 / 1.0$, are shown in figs. 8,9. Below the phase

transition one can set $d_0 = d_4 = 0$ and fit the potential with a simple quadratic form. This is not surprising

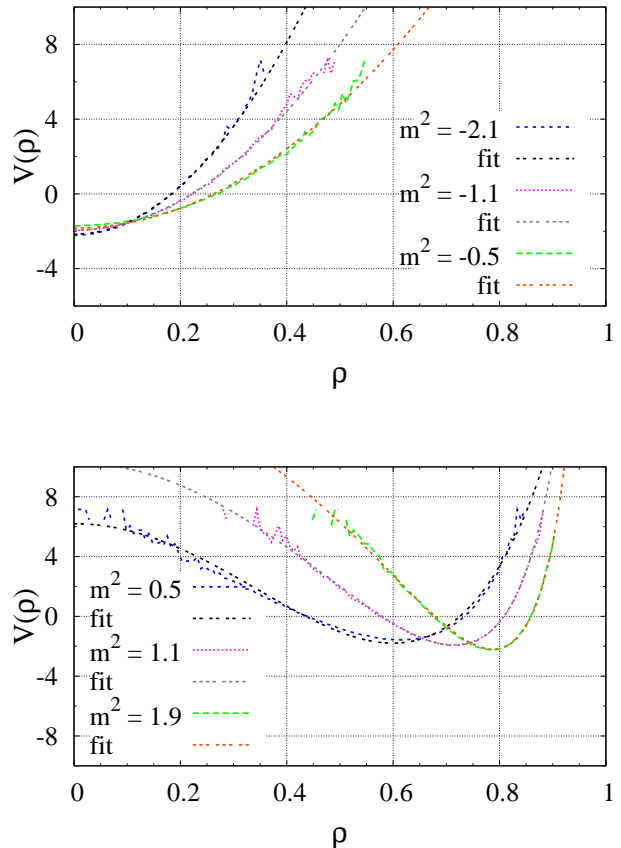


FIG. 8: The potential for blocks of side length $k = 3$ fit with ansatz (11) for $\beta = 1.0$ in confined (top) and deconfined (bottom) phases.

since for $\langle \ell \rangle = 0.0$ the potential is essentially parabolic and there is little sensitivity to higher powers of ℓ .

We show how the fit parameters from eq. (11) depend on β and m^2 . Figs. 10 and 12 correspond to $\beta = 1.0$ with variable m^2 and $m^2 = 0.0$ with variable β , respectively. One observes that right above the phase transition, the potential is a sum of quadratic and quartic terms while the Vandermonde contribution vanishes (in the figures, d_0 appears to fluctuate somewhat around zero. We have checked, however, that the result is consistent with setting $d_0 = 0$ by hand). At higher m^2 or β respectively, the coefficient d_0 increases gradually and saturates at about $d_0 \approx 80$ for large values of β or m^2 , while the quartic coefficient becomes negative. We have further checked that fixing d_0 to its asymptotic value ($d_0 \approx 80$) gives a less accurate fit and increases χ^2 per degree of freedom in the region closely above the phase transition roughly by a factor of two. This indicates that the gradual increase of d_0 is a real dynamical effect and not just an artifact generated by a lack of sensitivity to the Vandermonde

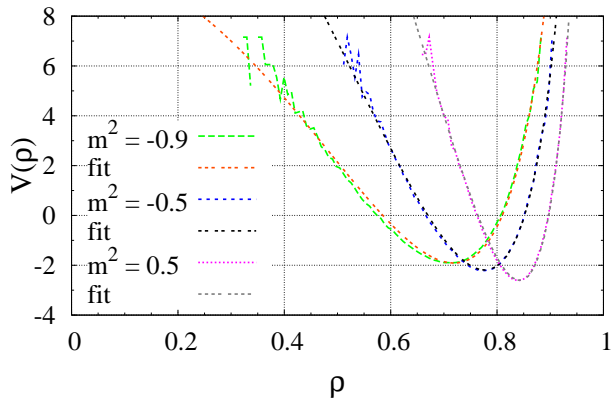
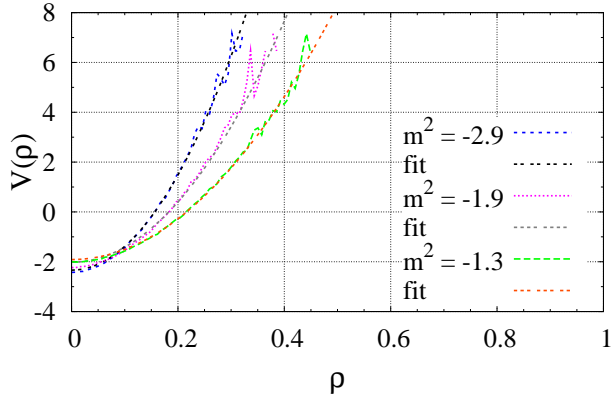


FIG. 9: The potential for blocks of side length $k = 3$ fit with ansatz (11) for $\beta = 2.0$ in confined (top) and deconfined (bottom) phases.

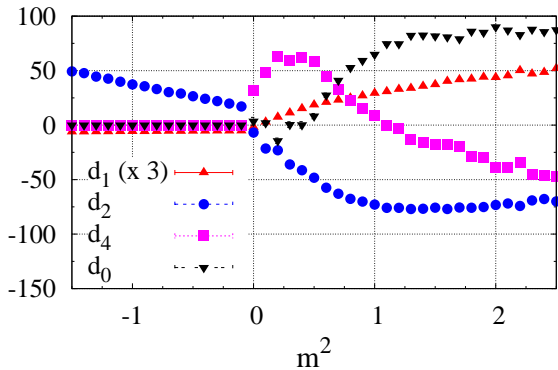


FIG. 10: The coefficients in eq. (11) for $\beta = 1.0$. The Vandermonde term appears to gradually rise to its asymptotic value.

potential when $\langle \rho \rangle$ is much smaller than 1. Fig. 11 shows that the region right above the phase transition, where the Vandermonde vanishes, appears to shrink when going

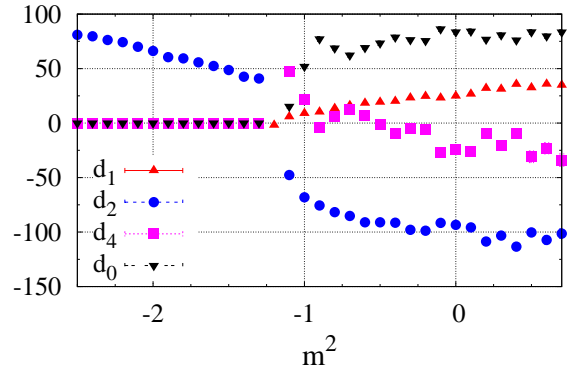


FIG. 11: The coefficients of eq. (11) $\beta = 2.0$. The region with vanishing Vandermonde term appears to shrink when going from $\beta = 1.0$ to $\beta = 2.0$. Compare to fig. 10

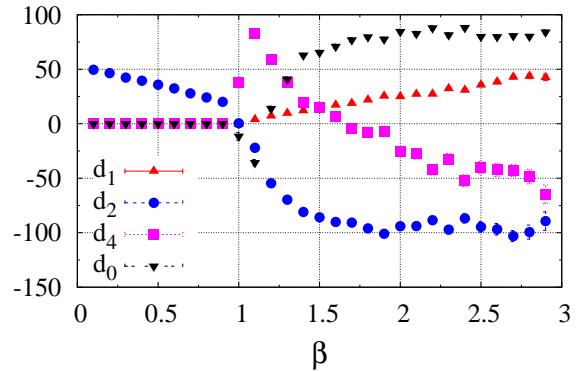


FIG. 12: A region with vanishing Vandermonde term is visible for $m^2 = 0.0$ and $\beta > \beta_C$.

deeper into the weak coupling limit (larger β).

The question remains, how this suppression of d_0 just above the phase transition, at moderately weak coupling, comes about. We have therefore attempted to model the potential right above the transition with a different function, assuming a fixed Vandermonde potential term, equal to the asymptotic value, but also allowing additional terms. We find that it is possible, within our numerical accuracy, to trade the suppression of the Vandermonde for another term linear in ρ . The function

$$V(\rho) = -d_0 \frac{1}{2} \log(1 - \rho^2) + d_1 + d'_0 \rho + d_2 \rho^2 + d_4 \rho^4, \quad \text{with } d_0 \approx 80, \quad (12)$$

reproduces the behavior of the effective potential around $\rho \approx 0.0$ even slightly better than eq. (11), with a negative coefficient d'_0 in the region right above the phase transition. However, the improvement in χ^2 is below the percent level and the function (12) fails completely

at large β or m^2 (by generating a potential that is not bounded from below).

The function (12) may suggest that the suppression of the Vandermonde could be an artifact due to incomplete cooling of short-distance fluctuations. However, we have investigated the cases [$\beta = 1.0/\text{variable } m^2$] and [$m^2 = 0.0/\text{variable } \beta$] also for $k = 4$ and obtained similar results, up to an overall scaling factor for all coefficients in the potential⁵. We show the result for $\beta = 1.0$ in fig. 13. Compared to fig. 10 we only observe a slight suppression of the quartic coefficient right above the phase transition.

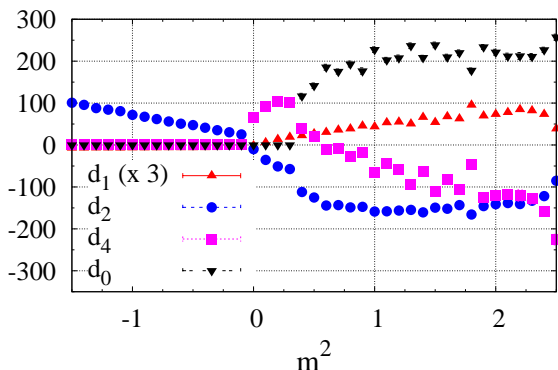


FIG. 13: The coefficients of eq. (11) for $\beta = 1.0$ at $k = 4$. Compare to fig. 10. For $m^2 \leq 0.3$ we set $d_0 = 0$ by hand (since in this region it yields no improvement of the goodness of the fit).

IV. SUMMARY AND DISCUSSION

We have performed simulations of an effective theory of Wilson lines coupled to gauge fields in three dimensions which respects the center symmetry of the four-dimensional SU(2) Yang-Mills theory. After mapping the phase diagram, we have investigated the effective potential for the average of the eigenvalues of the SU(2) Wilson line, which is equal to the absolute value of the Polyakov loop. We found that a form containing non-analytic contributions can describe the extracted potential. This non-analytic term was not present in the action, and therefore must arise from the dynamics.

We extracted a similar effective potential also for the long wavelength modes of the Polyakov loop and found

⁵ A rescaling of the coefficients in the potential is expected because coarse-graining over k lattice sites effectively corresponds to a simulation with different lattice spacing. A quantitative comparison of the coefficients of the $k = 3$ potential to those of the $k = 4$ potential would also require a rescaling of β .

that this can be described by a mean-field type potential with quadratic and quartic terms plus an effective Vandermonde potential which depends on the couplings. Just above the phase boundary, in the deconfined phase, the effective Vandermonde potential contributes little. Deeper into the deconfined phase its coefficient increases and eventually appears to approach a constant.

Our simulations may provide useful insight into the structure of mean-field type models for the deconfining phase transition. For example, so-called “Polyakov-NJL” models have recently been studied extensively. Such models attempt to describe QCD thermodynamics over a range of quark masses, from the pure-gauge limit to physical QCD; they require an *ansatz* for the effective potential for the Polyakov loop. For example, in early works on this subject [21] a quadratic potential for ℓ has been used, plus a Vandermonde contribution (per lattice site) which is constant and temperature independent. Our results appear to indicate, however, that if a standard potential with terms $\sim \ell^2$ and $\sim \ell^4$ (plus cubic Z(3) invariants for the case of three colors) is used, that a temperature dependent Vandermonde contribution should also be allowed for (this is already applied in some recent works, see e.g. ref. [22] and references therein). The present theory does not include fermions and so it is unfortunately not possible to address their effect. Nevertheless, PNJL models generally also include a pure loop potential, which describes the deconfining phase transition in the limit of infinitely heavy fermions.

Quantitative results for the physical case of three colors will of course differ, and indeed the order of the deconfining phase transition is different. Nevertheless, it appears hard to imagine that qualitative aspects, for example a temperature dependence of the effective Vandermonde term in the fitted effective potential, would be absent.

Acknowledgements

I am indebted to Adrian Dumitru, Rob Pisarski and Stefan Schramm for many helpful discussions. The numerical simulations presented here were performed at the Center for Scientific Computing (CSC) at Frankfurt University. Our code is based in part on the MILC collaboration’s public lattice gauge theory code, see <http://physics.utah.edu/~detar/milc.html>.

Appendix A: Coefficients in the effective potential for all modes

In this appendix we discuss the behavior of the non-analytic term in the potential defined in eq. (9) as a function of β and m^2 .

The case $m^2 = 0.0$ is rather simple. The nearly linear behavior of $b(\beta)$ above β_C , seen in Fig. 3 suggests an *ansatz* of the form

$$b(\beta) = b_0 (\beta - \beta_C)^r \theta(\beta - \beta_C) . \quad (\text{A1})$$

Indeed, we find that with $\beta_C = 0.9$, a good fit of $b(\beta)$ is possible, resulting in $b_0 = 7.1(1)$ and $r = 0.82(4)$. This fit corresponds to the solid line in fig. 3.

For $m^2 \neq 0.0$ the situation is more involved. As a heuristic analogy to the 2D Ising model we try the *ansatz*

$$b(\beta, m^2) = \tilde{b}(\beta) \theta(m^2 + \tilde{m}^2(\beta)) \times \left\{ 1 - \left[\sinh \left(2 \left[g(\beta) (m^2 + \tilde{m}^2(\beta)) + \tilde{\beta}_C \right] \right) \right]^{-5} \right\} \quad (\text{A2})$$

with $\tilde{\beta}_C = \log(1 + \sqrt{2})$ (see fig. 5). This is similar to the magnetization in the 2D Ising model [23], which is given by

$$M(\beta) = \theta(\beta - \tilde{\beta}_C) (1 - [\sinh(2\beta J)]^{-4})^{\frac{1}{8}}. \quad (\text{A3})$$

We find that (A2) works reasonably well for $\beta \leq 3.0$ (see the fit-curves in fig. 5 for specific examples). Note however that the exponents in eq. (A2) and eq. (A3) differ and that the *ansatz* (A2) does not imply any deeper connection from universality arguments. Once the β dependences of the parameters \tilde{m}^2 , g and \tilde{b} of eq. (A2) have been obtained it also describes $b(\beta, m^2 = 0)$, although less accurately than eq. (A1) since separate data sets (with fixed β and variable m^2) containing mostly measurements far from $m^2 = 0.0$ were used to obtain $\tilde{m}^2(\beta)$, $g(\beta)$ and $\tilde{b}(\beta)$. There is no straight-forward way to obtain eq. (A1) analytically from eq. (A2) and fitting (A2) directly to $b(\beta, m^2 = 0)$ is not feasible due to the large number of additional parameters that enter with the β dependence of \tilde{m}^2, g and \tilde{b} .

We have included the constant $\tilde{\beta}_C$ in eq. (A2) because it corresponds to the critical point of the Ising model. Our model of course deconfines at a different value of β . Nevertheless, an *ansatz* such as eq. (A3) implicitly assigns the number $\tilde{\beta}_C$ a special meaning and we therefore include it into our *ansatz* also in order to “filter out” its effect. Isolating $\tilde{\beta}_C$ in such a way simplifies the resulting dependence of the fit parameters on β greatly.

The coefficients introduced in eq. (A2) act as follows: \tilde{m}^2 corresponds to a shift along the horizontal axis. \tilde{b} is a scaling factor and g is a modification of the coupling strength. The β dependence of these coefficients can be described by power laws

$$\tilde{m}^2(\beta) = m_0^2 + m_0'^2 \beta^w, \quad (\text{A4})$$

$$\tilde{b}(\beta) = b_0' + b_0'' \beta^v, \quad (\text{A5})$$

$$g(\beta) = g_0 + g_0' \beta^u, \quad (\text{A6})$$

with

$$m_0^2 = 2.2(1), \quad m_0'^2 = -2.1(1), \quad w = -1.2(1), \quad (\text{A7})$$

$$b_0' = -2.5(4), \quad b_0'' = 6.0(4), \quad v = 0.90(4), \quad (\text{A8})$$

$$g_0 = 0.038(1), \quad g_0' = 0.017(1), \quad u = 2.8(1). \quad (\text{A9})$$

The β dependence of \tilde{m}^2 , \tilde{b} and g is shown in fig. 14.

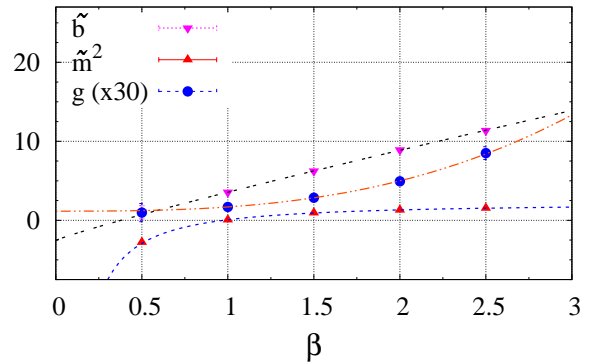


FIG. 14: β dependence of various coefficients parameterizing $b(\beta, m^2)$ with their corresponding fit curves. $g(\beta)$ is scaled up by a factor of 30.

Appendix B: First-order transition in extreme weak coupling limit

At very large β the transition becomes first order. To see this, consider figs. 15 and 16. For $\beta = 5.0$ the effective potential develops two distinct minima in the vicinity of the phase transition point. Correspondingly, the Polyakov loop expectation value appears to be discontinuous. This behavior is in sharp contrast to the case

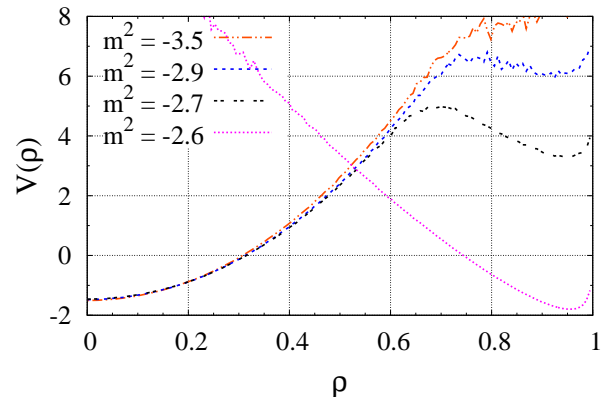


FIG. 15: Effective potential for $\beta = 5.0$ at values of m^2 slightly above and slightly below the phase transition. A first order phase transition is apparent since one observes two distinct minima.

$\beta = 2.0$ (shown in fig. 4), where one can see a single minimum moving continuously with m^2 (within the resolution) from $\rho \approx 0$ to $\rho \approx 1$.

The first order transition indicates that our effective theory cannot describe 4D Yang Mills when β is too large. This is not problematic however, since the coupling constant β in the effective theory is unrelated to

the 4D case. When matching the theories, any value of β in the 4D SU(2) Yang Mills theory close to the second order phase transition will correspond to a combination of coupling constants in the effective theory in the vicinity of the second order phase boundary. While it may be necessary to include higher powers of the Polyakov loop and additional coupling constants to the action (5) to make a precise matching possible (there is also no ad hoc justification for the assumption that the coupling constants of the kinetic energy term and of the 3D Wilson action of the spatial gauge fields must be the same), the presence of a first order phase boundary in the parameter space of the effective theory is itself of no relevance to the matching procedure.

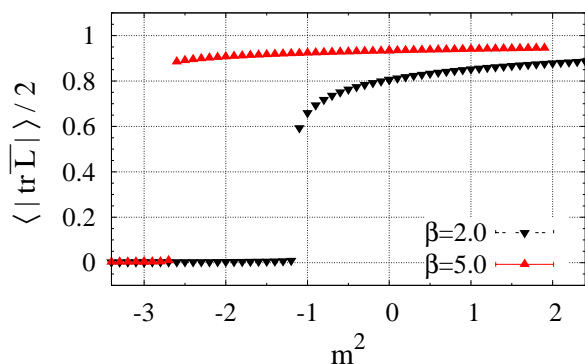


FIG. 16: Polyakov Loop expectation value for $\beta = 2.0$ and $\beta = 5.0$ measured on $N_s = 24$. The transition becomes very sharp for large β .

- [1] see, for example, J. O. Andersen and M. Strickland, *Annals Phys.* **317**, 281 (2005) [arXiv:hep-ph/0404164]; J. O. Andersen, M. Strickland and N. Su, arXiv:0911.0676 [hep-ph]; Y. Schröder, *PoS JHW2005*, 029 (2006) [arXiv:hep-ph/0605057]; J. P. Blaizot, *Nucl. Phys. A* **785**, 1 (2007) [arXiv:nucl-th/0611104]; and references therein.
- [2] R. D. Pisarski, *Phys. Rev. D* **62**, 111501 (2000) [arXiv:hep-ph/0006205]; A. Dumitru, J. Lenaghan and R. D. Pisarski, *Phys. Rev. D* **71**, 074004 (2005); A. Dumitru, R. D. Pisarski and D. Zschiesche, *Phys. Rev. D* **72**, 065008 (2005);
- [3] A. Dumitru, Y. Hatta, J. Lenaghan, K. Orginos and R. D. Pisarski, *Phys. Rev. D* **70**, 034511 (2004);
- [4] P. N. Meisinger, T. R. Miller and M. C. Ogilvie, *Phys. Rev. D* **65**, 034009 (2002) [arXiv:hep-ph/0108009]; P. N. Meisinger, M. C. Ogilvie and T. R. Miller, *Phys. Lett. B* **585**, 149 (2004) [arXiv:hep-ph/0312272].
- [5] R. D. Pisarski, *Phys. Rev. D* **74**, 121703 (2006) [arXiv:hep-ph/0608242].
- [6] A. Vuorinen and L. G. Yaffe, *Phys. Rev. D* **74**, 025011 (2006) [arXiv:hep-ph/0604100]; A. Kurkela, arXiv:0704.1416 [hep-lat]; Ph. de Forcrand, A. Kurkela and A. Vuorinen, *Phys. Rev. D* **77**, 125014 (2008) [arXiv:0801.1566 [hep-ph]].
- [7] O. Kaczmarek, F. Karsch, P. Petreczky and F. Zantow, *Phys. Lett. B* **543**, 41 (2002) [arXiv:hep-lat/0207002]; S. Gupta, K. Hübner and O. Kaczmarek, *Nucl. Phys. A* **785**, 278 (2007) [arXiv:hep-lat/0608014]; O. Kaczmarek, S. Gupta and K. Hübner, arXiv:0710.2277 [hep-lat].
- [8] D. J. Gross, R. D. Pisarski and L. G. Yaffe, *Rev. Mod. Phys.* **53**, 43 (1981).
- [9] E. Megias, E. Ruiz Arriola and L. L. Salcedo, *JHEP* **0601**, 073 (2006) [arXiv:hep-ph/0505215]; *Phys. Rev. D* **74**, 114014 (2006) [arXiv:hep-ph/0607338]; *Phys. Rev. D* **75**, 105019 (2007) [arXiv:hep-ph/0702055]; *Phys. Rev. D* **80**, 056005 (2009) [arXiv:0903.1060 [hep-ph]]; Y. Hidaka and R. D. Pisarski, *Phys. Rev. D* **78**, 071501 (2008) [arXiv:0803.0453 [hep-ph]]. *Phys. Rev. D* **80**, 036004 (2009) [arXiv:0906.1751 [hep-ph]]. *Phys. Rev. D* **80**, 074504 (2009) [arXiv:0907.4609 [hep-ph]].
- [10] C. P. Korthals Altes, *Nucl. Phys. A* **820**, 219C (2009) [arXiv:0810.3325 [hep-ph]].
- [11] L. Dittmann, T. Heinzl and A. Wipf, *JHEP* **0406**, 005 (2004) [arXiv:hep-lat/0306032]; T. Heinzl, T. Kaestner and A. Wipf, *Phys. Rev. D* **72**, 065005 (2005) [arXiv:hep-lat/0502013]; C. Wozar, T. Kaestner, A. Wipf, T. Heinzl and B. Pozsgay, *Phys. Rev. D* **74**, 114501 (2006) [arXiv:hep-lat/0605012]; A. Velytsky, *Phys. Rev. D* **78**, 034505 (2008) [arXiv:0805.4450 [hep-lat]].
- [12] A. Hietanen and A. Kurkela, *JHEP* **0611**, 060 (2006) [arXiv:hep-lat/0609015].

- [13] A. Dumitru and D. Smith, Phys. Rev. D **77**, 094022 (2008); D. Smith, Nucl. Phys. A **820**, 227 (2009) [arXiv:0810.1129 [hep-lat]].
- [14] A. Guha and S. C. Lee, Nucl. Phys. B **240** (1984) 141; P. Dreher, Phys. Lett. B **281** (1992) 127.
- [15] J. B. Kogut, M. Snow and M. Stone, Nucl. Phys. B **200**, 211 (1982).
- [16] M. Creutz, Phys. Rev. D **36**, 515 (1987). F. R. Brown and T. J. Woch, Phys. Rev. Lett. **58** (1987) 2394.
- [17] A. Velytsky, Int. J. Mod. Phys. C **19** (2008) 1079 [arXiv:0711.0748 [hep-lat]].
- [18] B.A. Berg, “Markov Chain Monte Carlo Simulations and Their Statistical Analysis”, World Scientific, 2004.
- [19] J. C. Myers and M. C. Ogilvie, Nucl. Phys. A **820**, 187C (2009) [arXiv:0810.2266 [hep-th]]; J. C. Myers and M. C. Ogilvie, arXiv:0809.3964 [hep-lat].
- [20] B. Svetitsky and L. G. Yaffe, Nucl. Phys. B **210**, 423 (1982).
- [21] K. Fukushima, Phys. Lett. B **591**, 277 (2004) [arXiv:hep-ph/0310121].
- [22] T. Hell, S. Rossner, M. Cristoforetti and W. Weise, arXiv:0911.3510 [hep-ph].
- [23] R. Fiore, F. Gliozzi and P. Provero, Phys. Rev. D **58**, 114502 (1998) [arXiv:hep-lat/9806017].